

## Comparison of the Dynamics of Particles in a Flow Field with the Reynolds and Favre Filtered Flow Velocities.

P. C. Stegeman<sup>1</sup>, J. Soria<sup>1,2</sup> and A. Ooi<sup>3</sup>

<sup>1</sup>Laboratory for Turbulence Research in Aerospace and Combustion, Department of Mechanical and Aerospace Engineering, Monash University, VIC 3800, AUSTRALIA

<sup>2</sup>Department of Aeronautical Engineering, King Abdulaziz University, Jeddah, Kingdom of Saudi Arabia

<sup>3</sup>Department of Mechanical Engineering, University of Melbourne, Parkville, VIC 3052, AUSTRALIA

### Abstract

A parametric study has been undertaken using direct numerical simulations (DNS) of forced compressible particle-laden flow in order to determine the validity of the comparison between PIV flow fields and LES Reynolds/Favre filtered flow fields. This requires solving the 3D Navier-Stokes equations and particle dynamics in a periodic domain where important parameters include the Reynolds number, Mach number, Particle diameter, filter width and ratio of solenoidal to dilatational dissipation. Tentative results of the simulations are presented.

### Introduction

The Reynolds filtering and Favre filtering techniques are commonly used to filter velocity fields in compressible large-eddy simulations (LES). LES solves a filtered version of the Navier-Stokes equations so that it may differentiate between the turbulent scales that are resolvable by the mesh and the sub-grid scales that cannot be resolved and therefore are required to be modeled. The filtering operation in LES is generally done via the spatial convolution

$$\bar{\phi}(\mathbf{x}) = \int_{-\infty}^{\infty} \int_{-\infty}^{\infty} \int_{-\infty}^{\infty} G\left(\frac{\mathbf{x}-\xi}{\Delta}\right) \phi(\xi) d^3\xi \quad (1)$$

where  $G$  is the filter function and  $\Delta$  is the cut-off spatial scale while  $\phi(\xi)$  and  $\bar{\phi}(\mathbf{x})$  represents a unfiltered and filtered variable in space. In Reynolds averaged LES the filtered velocity is determined via the direct application of equation 1 producing

$$u_i = \bar{u}_i + u'_i \quad (2)$$

where  $\bar{u}_i$  is the filtered velocity term and  $u'_i$  is the sub-grid velocity term. In contrast, Favre averaging is defined as

$$u_i = \frac{\bar{\rho u_i}}{\bar{\rho}} + u''_i = \tilde{u}_i + u''_i \quad (3)$$

where  $\tilde{u}_i$  is the filtered velocity term and  $u''_i$  is the sub-grid velocity term. For compressible flows  $\tilde{u}_i \neq \bar{u}_i$  and Favre averaging is generally used due to the reduction in the number of subgrid scale terms that need to be modeled.

Particle image velocimetry (PIV) determines a flow's velocity field by cross-correlating the positions of groups particles within the flow across time samples. Panda *et al.* [9] and Garnier *et al.* [5] both state that PIV produces Reynolds averaged velocity fields. However no quantitative analysis or proof of this can be found in current literature. To establish similarity with a well designed PIV experiment only particles with small Stokes numbers and

therefore small diameters are considered. The average acceleration of a small particle due to local Stokes drag is defined by Varaksin [14] as

$$\frac{\partial u_{p_i}}{\partial t} = \frac{w_i}{\tau_p} \quad (4)$$

where  $\tau_p$  is the relaxation time of the particle,  $u_{p_i}$  is the particle velocity and  $w_i$  is the velocity of the carrier fluid at the particles position. If  $\tau_p$  remains constant (The particle Stokes number  $Stk_p \ll 1$ ) then it would be expected that the particle follows the Reynolds averaged velocity field due to the lack of dependency on the carrier fluid's density. However in general  $\tau_p$  will fluctuate as the particle travels and is dependent on the carrier fluid's thermodynamic properties. It is therefore important to understand the difference between the dynamics of a particle in an unfiltered compressible flow field and the Reynolds/Favre filtered flow velocity at the particle's position. In this study a parametric analysis is undertaken at a variety of fluid and particle conditions in order to gain a basic understanding of the validity of comparing Reynolds and Favre averaged velocity fields with those found experimentally using particle image velocimetry.

### Governing Equations and Numerical Methods

#### Fluid Dynamics

The continuity, momentum and energy equations that govern turbulent compressible flow in non-dimensional form are

$$\begin{aligned} \frac{\partial \rho}{\partial t} + \frac{\partial \rho u_j}{\partial x_j} &= 0 \\ \frac{\partial \rho u_i}{\partial t} + \frac{\partial \rho u_i u_j}{\partial x_j} + \frac{\partial p}{\partial x_j} &= \frac{\partial \tau_{ij}}{\partial x_j} + f_i \\ \frac{\partial E}{\partial t} + \frac{\partial u_j(E+p)}{\partial x_j} &= \frac{\partial (u_i \tau_{ij})}{\partial x_j} - \frac{\partial q_j}{\partial x_j} + u_i f_i + f_e \end{aligned}$$

where  $\rho$  is the density,  $u_i$  the velocity vector,  $E$  the total energy,  $p$  the pressure,  $\tau_{ij}$  the stress tensor,  $q_i$  the heat flux and  $f_i$  the forcing acting on the fluid. In this analysis the internal energy forcing  $f_e$  is assumed to be  $f_e = -u_i f_i$  such that for homogeneous turbulence the total energy will remain constant. The stress tensor and heat flux are defined as

$$\begin{aligned} \tau_{ij} &= \frac{\mu}{Re_0} \left( \frac{\partial u_i}{\partial x_j} + \frac{\partial u_j}{\partial x_i} - \frac{2}{3} \frac{\partial u_k}{\partial x_k} \delta_{ij} \right) \\ q_j &= \frac{\gamma \mu}{\gamma - 1} \frac{1}{M_0^2 Pr} \frac{\partial T}{\partial x_j} \end{aligned}$$

where the reference Mach number  $M_0 = u_0 / \sqrt{RT_0}$ , in which  $R$  is the gas constant, the reference Reynold's number  $Re_0 = \rho_0 L_0 u_0 / \mu_0$  and  $Pr$  is the Prandtl number. The variables in these equations have been non dimensionalized by the reference values  $L_0$  for length,  $u_0$  for velocity,  $\rho_0$  for density,  $L_0/u_0$  for time,  $T_0$  for temperature,  $\mu_0$  for viscosity and  $\rho_0 u_0^2$  for pressure and energy. For an ideal gas the equation of state and total energy are defined as

$$p = \frac{\rho T}{M_0^2}$$

$$E = \frac{\rho u_i u_i}{2} + \frac{\rho T}{(\gamma - 1) M_0^2}.$$

Consistent reference parameters and relationships defined for this analysis are  $T_0 = 288.15\text{K}$ ,  $R = 287\text{J}\cdot\text{kg}^{-1}\text{K}^{-1}$ ,  $Pr = 0.7$  and  $\mu = T^{0.76}$ . Two important statistical quantities of homogeneous and isotropic turbulence are the turbulent Mach number

$$M_t = M_0 \frac{u_{rms}}{\langle \sqrt{\gamma T} \rangle} \quad (5)$$

and the Taylor Reynolds number

$$Re_\lambda = Re_0 \frac{\langle \rho \rangle \lambda u_{rms}}{\langle \mu \rangle} \quad (6)$$

where  $u_{rms} = \sqrt{u_i u_i / 3}$  and  $\lambda = (1/3) \sum_{i=0}^3 \sqrt{u_i / (\partial u_i / \partial x_i)}$ .

To maintain a statistically stationary turbulent Mach number and Taylor Reynolds number the partial wavenumber forcing methodology of Petersen and Livescu [10] is used. Forcing is applied separately to the solenoidal and dilatational velocity fields in the wavenumber band between  $0 \leq \mathbf{k} < \sqrt{6}$ . This allows the statistical average solenoidal dissipation ( $\epsilon_{s_{target}}$ ) and dilatational dissipation ( $\epsilon_{d_{target}}$ ) to be controlled. To reduce the number of simulation parameters the model  $\epsilon_{s_{target}} / \epsilon_{d_{target}} \approx \alpha_1 M_t^2$  proposed by Sarkar *et al.* [12] is used. From DNS simulations [12] and [3] found that  $\alpha_1 = 1.0$  provides a reasonable fit for isotropic turbulence and is the value used for all simulations. It should be noted however that [8] describes uncertainty of  $\alpha_1$  with respect to flow structure giving a range of  $0.5 \leq \alpha_1 \leq 1.0$  for homogeneous shear flows at low Reynolds numbers. The total dissipation,  $\epsilon_{target} = \epsilon_{s_{target}} + \epsilon_{d_{target}}$ , is determined by the target Kolmogorov scale where  $\eta_{target} = (v^3 / \epsilon_{target})^{1/4}$ .

The initial solenoidal velocity field is generated via the methodology in Blaisdell [2] with an initial kinetic energy spectrum

$$E(k) = 16 u_{rms}^2 \sqrt{\frac{2}{\pi}} \frac{k^4}{k_0^5} e^{-2k^2/k_0^2} \quad (7)$$

where  $k_0 = 2/\lambda_0$  is the most energetic wavenumber. The initial dilatational velocity, pressure fluctuations and density fluctuations are calculated using the method by Ristorcelli and Blaisdell [11]. This method is only valid for nearly incompressible flow therefore if  $M_{t_{target}} > 0.1$  the initial velocity fluctuations are reduced such that  $M_t = 0.1$  and the target turbulent Mach number is reached through forcing of the flow.

The numerical methodology for the fluid phase is based on the Hybrid method in Johnsen *et al.* [7]. For convective terms 6th and 10th order central differencing schemes are used in smooth regions of the flow while Roe flux-splitting

with 5th order WENO interpolation as defined by Shu [13] is used in discontinuous regions of the flow. The regions are determined by the shock-sensor developed by Ducros *et al.* [4]. In the smooth regions all non-linear terms are calculated in their conservative split-form equivalent to method E in [2]. In discontinuous regions the viscous fluxes are calculated in their non-conservative form. Time integration is performed using the 3rd order TVD Runge-Kutta defined by Gottlieb *et al.* [6].

For general LES simulations, such as those employing the Smagorinsky, structure function, or dynamic sub-grid scale models; no explicit filtering is applied to the fluid state. Instead the grid acts as an ideal filter with a cutoff wavenumber equal to its Nyquist wavenumber such that

$$\hat{G}(k) = \begin{cases} 1 & k \leq k_{max} \\ 0 & k > k_{max} \end{cases} \quad (8)$$

where  $\hat{G}$  is the filter function in wavenumber space and  $k_{max}$  is the Nyquist (maximum) wavenumber of the grid. Therefore to generate the Reynolds and Favre filtered velocities an ideal low-pass filter with a Blackmann window is used. The discrete representation of this filter is

$$\bar{\phi}(x) = \sum_{i=-N/2}^{N/2} \underbrace{N \frac{\sin\left(\pi \frac{(k\Delta)_f i}{N}\right)}{\pi i}}_{\text{Ideal Filter}}$$

$$\underbrace{\left[ 0.4266 + 0.4966 \cos\left(\frac{2\pi i}{N}\right) + 0.0768 \cos\left(\frac{4\pi i}{N}\right) \right]}_{\text{Blackman Window}} \quad (9)$$

$$\phi(x + \Delta i)$$

where  $N + 1$  is the filter width and  $(k\Delta)_f$  is the cutoff wavenumber ratio. For all simulations the filter width is set to 41 and the cutoff ratio  $(k\Delta)_f = 0.2$  such that the ideal cutoff wavenumber is 20% of the grid's Nyquist wavenumber. By setting  $(k\Delta)_f$  to a constant value the size of the parametric space is reduced.

### Particle Dynamics

The Stokes number of a particle is defined as

$$Stk_p = \frac{\tau_p}{\tau_f} \quad (10)$$

where  $\tau_p$  is the relaxation time of the particle and  $\tau_f$  is a characteristic timescale of the carrier fluid which is taken to be the eddy turnover time  $\tau_f = \lambda / u_{rms}$ . It is assumed in this analysis that the particle's diameter is small in comparison with the velocity fluctuations of the carrier fluid that contain a majority of the turbulent kinetic energy. Therefore the magnus, turbophoresis and thermophoresis forces are considered small enough relative to the aerodynamic drag such that they can be safely ignored. The dimensionless particle relaxation time due to Stokes drag is derived from Varaksin [14] as

$$\tau_p = Re_0 \frac{\rho_p d_p^2}{18 \mu C} \quad (11)$$

where the particle's Reynolds number is

$$Re_p = Re_0 \frac{\rho \sqrt{w_i w_i} d_p}{\mu} \quad (12)$$

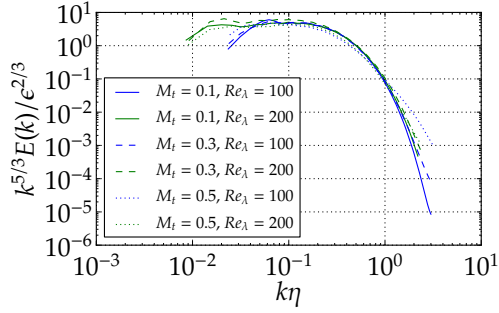


Figure 1: Normalized kinetic energy spectra.

and  $C = 1 + 0.15Re_p^{0.687}$  is the Schiller-Naumann correction factor. For homogeneous isotropic turbulence there is no Staffman force acting on the particle due to the lack of mean velocity gradients in the flow. A review by Balachandar *et al.* [1] confirmed that for small particles in isotropic turbulence Equation 11 is sufficiently accurate. It is also assumed that the particle density is equivalent to the fluid density such that the buoyancy and gravitational forces can be ignored. This is a reasonable assumption for comparison with PIV experiments in which the seeding particles are chosen such that their density are as close to the working fluid's as possible.

High-order spline interpolation is used to determine the fluid state at each particles' position. The spline polynomial is of degree 22 which provides an relative accuracy of at least 99% for wavenumbers below half the Nyquist limit. Interpolation of a 3D function is determined via successive 1D interpolations of the required grid points along each axis.

### Simulation Methodology and Parameters

In order to conserve computational resources the simulations are initial run on a low quality grid until the flow has achieved a statistically stationary state. All simulation reached a statistically stationary state within 150 to 250 eddy turn-over times. The state fields are then spectrally interpolated to a larger grid such that  $k_e\eta > 1.5$  where  $k_e$  is the computational wavenumber for which the error in relative wavenumber due to the central differencing scheme is  $\approx 10\%$ . The simulation statistics and parameters for each of the test cases can be seen in Table 1. The normalized kinetic energy spectra for each of the cases may be seen in Figure 1. Based on the kinetic energy spectra the spline interpolation of the velocity field has an absolute error of  $\approx 10^{-6}$ .

For each test case 8192 particles were simulated at relative diameters of  $d/L_0 = 0.05, 0.1, 0.2$ . Initially the particles are uniformly distributed across the domain with an initial velocity equal to the flow velocity at their respective positions. Due to the large time iteration constraints posed by the particles with small diameters ( $\Delta t \propto d^{-2}$ ) each test case has currently only achieved a simulation time of approximately 0.5 eddy turn-over times such that the current results presented should be read as tentative.

### Results and Analysis

The relative difference in velocity  $u_e$  between the particle velocity ( $\mathbf{u}_p$ ) and flow velocity ( $\mathbf{u}_\phi$ ) at the particle's

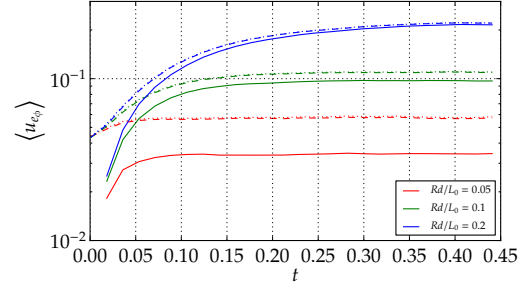


Figure 2: Average error of particle velocity with respect to the unfiltered, Reynolds filtered and Favre filtered flow velocities for the simulation  $M_{t,target} = 0.5$ ,  $Re_{\lambda,target} = 200$ . Solid lines represent the unfiltered error ( $\phi = u$ ), dashed lines represent the Reynolds filtered error ( $\phi = r$ ) and the dotted lines represent the Favre filtered error ( $\phi = f$ ).

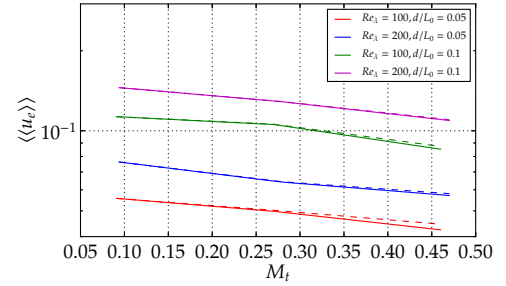


Figure 3: Ensemble averaged error of particle velocity with respect to the unfiltered, Reynolds filtered and Favre filtered flow velocities as a function of Mach number. Solid lines represent the unfiltered error ( $\phi = u$ ), dashed lines represent the Reynolds filtered error ( $\phi = r$ ) and the dotted lines represent the Favre filtered error ( $\phi = f$ ).

position ( $\mathbf{x}_p$ ) is defined as

$$u_{e\phi} = \left| \mathbf{u}_p - \mathbf{u}_\phi(\mathbf{x}_p) \right| / \left| \mathbf{u}_u(\mathbf{x}_p) \right| \quad (13)$$

where  $\phi = u$  represents the unfiltered flow velocity,  $\phi = r$  represents the Reynolds filtered flow velocity and  $\phi = f$  represents the Favre filtered flow velocity. The average of  $u_e$  is shown for a single test case in Figure 2. As may be seen the time it takes for  $u_e$  to reach a relatively steady state increases with respect to the particle diameter and is due to the larger relaxation times of larger particles. The larger relaxation time also increases the average of  $u_e$  due to the particles' decreased response to velocity fluctuations. To understand the relationship between  $u_e$  and simulation parameters  $Re_\lambda$  and  $M_t$  Figure 3 plots the ensemble average ( $\langle\langle \rangle\rangle$ ) for eddy turnover times  $t > 0.3$  for each test case. As expected  $\langle\langle u_e \rangle\rangle$  increases with increasing particle diameter and  $Re_\lambda$ . However the decrease in  $\langle\langle u_e \rangle\rangle$  with increasing Mach number is unexpected and its cause is currently being investigated. Figure 4 plots the difference  $\delta\langle\langle u_e \rangle\rangle = \left| \langle\langle u_{er} \rangle\rangle - \langle\langle u_{ef} \rangle\rangle \right|$  between the Reynolds and Favre filtered results in Figure 3. For both Reynolds and Favre filtered flow velocities  $\delta\langle\langle u_e \rangle\rangle$  increases with Mach number as is expected due to the increasing density fluctuations. However for moderate values of  $M_t$  the differences between the two filtering regimes is insignificant ( $< 0.3\%$ ).

$M_{t,target}$	$Re_{\lambda,target}$	Low Quality Grid Size	High Quality Grid Size	$\langle Re_{\lambda} \rangle$	$\langle M_t \rangle$	$\langle \eta \rangle (10^{-3})$	$\langle \lambda \rangle$	$\langle L \rangle$	% $E(k)$ between $0 \leq k\Delta < 0.2$
0.1	100	125 <sup>3</sup>	256 <sup>3</sup>	84 ± 10	0.091 ± 0.004	51 ± 2.5	0.93 ± 0.097	13.3	99.7
0.1	200	125 <sup>3</sup>	512 <sup>3</sup>	210 ± 32	0.094 ± 0.003	39 ± 2.5	1.11 ± 0.16	26.7	99.4
0.3	100	125 <sup>3</sup>	256 <sup>3</sup>	84 ± 12	0.27 ± 0.012	52 ± 2.7	0.92 ± 0.11	13.3	99.7
0.3	200	125 <sup>3</sup>	512 <sup>3</sup>	231 ± 33	0.28 ± 0.016	42 ± 1.5	1.24 ± 0.12	26.7	99.6
0.5	100	125 <sup>3</sup>	256 <sup>3</sup>	86 ± 16	0.46 ± 0.04	54 ± 2.9	0.94 ± 0.11	13.3	99.7
0.5	200	243 <sup>3</sup>	512 <sup>3</sup>	200 ± 32	0.47 ± 0.03	40 ± 1.5	1.07 ± 0.11	26.6	99.5

Table 1: Test cases' parameters and statistics. The ensemble averaged ( $\langle \rangle$ ) quantities are given along side their range defined as  $\pm 3$  standard deviations.  $L$  denotes the domain size.

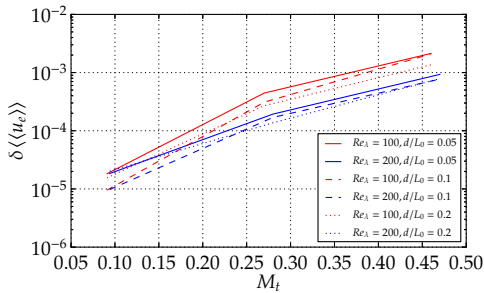


Figure 4: Difference of the ensemble averaged error between the particles' velocities with respect to the Reynolds filtered flow velocities and error between the particles' velocities with respect to the Favre filtered flow velocities as a function of Mach number.

## Conclusions

Initial simulations of particle-laden compressible turbulent flow has been completed to determine the validity of the comparison between PIV flow fields and LES Reynolds/Favre filtered flow fields. From the initial results the difference between the different filtering regimes is found to be small with respect to the velocity induced by the particles' dynamics. For real PIV experiments the difference is likely to be smaller than the measurement uncertainty. However the statistics measuring the difference in velocity have not yet been determined to a sufficient accuracy to make reasonable judgments from the data. Simulations are continuing with a wider parametric space that will allow for definitive conclusions to be drawn.

## Acknowledgements

P. C. Stegeman would like to acknowledge ARC for supporting his candidature for Doctor of Philosophy and the National Computational Infrastructure for supplying the required computational resources.

## References

- [1] Balachandar, S. and Eaton, J. K., Turbulent dispersed multiphase flow, *Annual Review of Fluid Mechanics*, **42**, 2010, 111–133.
- [2] Blaisdell, G. A., *Numerical simulation of compressible homogenous turbulence*, Ph.D. thesis, Stanford University, 1991.
- [3] Blaisdell, G. A., Mansour, N. N. and Reynolds, W. C., Numerical simulation of compressible homogenous

turbulence, Technical Report TF-50, Themosci. Div., Mech. Engrg., Stanford University, 1992.

- [4] Ducros, F., Ferrand, V., Nicoud, F., Weber, C., Darzacq, D., Gacherieu, C. and Poinot, T., Large-eddy simulation of the shock/turbulence interaction, *Journal of Computational Physics*, **152**, 1999, 517–549.
- [5] Garnier, E., Adams, N. and Sagaut, P., *Large Eddy Simulation for Compressible Flows*, Springer, 2009.
- [6] Gottlieb, S. and Shu, C.-W., Total variation diminishing runge-kutta schemes, *Mathematics of Computation*, **67**, 1998, 73–85.
- [7] Johnsen, E., Larsson, J., Bhagatwala, A. V., Cabot, W. H., Moin, P., Olson, B. J., Rawat, P. S., Shankar, S. K., Sjogreen, B., Yee, H. C., Zhong, X. and Lele, S. K., Assessment of high-resolution methods for numerical simulations of compressible turbulence with shock waves, *Journal of Computational Physics*, **229**, 2010, 1213–1237.
- [8] Lele, S. K., Compressibility effects on turbulence, *Annual Review of Fluid Mechanics*, **26**, 1994, 211–254.
- [9] Panda, J. and Seasholtz, R. G., Experimental investigation of reynolds and favre averaging in high speed jets, *AIAA Journal*, **44**, 2006, 1952–1959.
- [10] Petersen, M. R. and Livescu, D., Forcing for statistically stationary compressible isotropic turbulence, *Physics of Fluids*, **22**, 2010, 116101.
- [11] Ristorcelli, J. R. and Blaisdell, G. A., Consistent initial conditions for the dns of compressible turbulence, *Physics of Fluids*, **9**, 1997, 4.
- [12] Sarkar, S., Erlebacher, G., Hussaini, M. Y. and Kreiss, H. O., The analysis and modelling of dilatational terms in compressible turbulence, *Journal of Fluid Mechanics*, **227**, 1991, 473–493.
- [13] Shu, C.-W., Efficient implementation of essentially non-oscillatory shock-capturing schemes, *Journal of Computational Physics*, **77**, 1988, 439–471.
- [14] Varaksin, A. Y., *Turbulent Particle-Laden Gas Flows*, Springer-Verlag, 2007.